Physics-Driven Machine-Learning Approach Incorporating Temporal Coupled Mode Theory for Intelligent Design of Metasurfaces

Jianan Zhang, *Member, IEEE*, Jian Wei You, *Senior Member, IEEE*, Feng Feng, *Senior Member, IEEE*, Weicong Na, *Member, IEEE*, Zhuo Chen Lou, *Graduate Student Member, IEEE*, Qi-Jun Zhang, *Fellow, IEEE*, and Tie Jun Cui, *Fellow, IEEE*

***Abstract*— Metasurfaces find a wide variety of applications in the last decades due to their powerful ability to manipulate electromagnetic (EM) waves. Traditional approaches for metasurface design require massive full-wave EM simulations to achieve optimal geometrical parameter values, resulting in an inefficient design process of metasurfaces. In this article, we propose a physics-driven machine-learning (ML) approach incorporating temporal coupled mode theory (CMT) to improve the design efficiency and implement an intelligent design of metasurfaces. In the proposed approach, a surrogate model (i.e., neuro-CMT model) is developed to speed up the prediction of EM responses of metasurfaces. A three-stage method is used to develop the neuro-CMT model. First, we perform full-wave EM simulations of unit cells only containing single- and double-resonators for different geometrical design parameter values. Second, we extract the single- and double-resonator CMT parameters for each geometrical parameter value by fitting the corresponding EM responses based on CMT equations. Third, we train neural networks to learn the relationships between the CMT parameters and geometrical parameters for single- and double-resonator systems, respectively. These trained neural networks, in conjunction with the multiresonator CMT equation, become an efficient tool to accurately predict the EM responses of any arbitrary coupled multiresonator systems. The proposed neuro-CMT model can be further utilized for metasurface design optimizations. Two metasurface absorbers are given as examples to demonstrate the efficient and intelligent advantages of our proposed approach.**

***Index Terms*— Electromagnetic (EM) parametric modeling, EM optimization, metasurface design, physics-driven machine-learning (ML), temporal coupled mode theory (CMT).**

I. Introduction

THE last decade has witnessed the advances of metasurfaces in a wide variety of applications [1], [2], [3]. Due to their powerful ability to manipulate electromagnetic (EM) waves, metasurfaces are deemed one of the most promising technologies for next-generation communication systems.

One crucial, yet challenging task in metasurface design is parametric optimization, that is, finding the optimal set of geometrical/structural parameter values with desired EM responses. Traditionally, this task is fulfilled by applying the optimization subroutine in commercial EM simulation software, where massive full-wave EM simulations have to be performed with repetitively changed geometrical parameter values. This traditional method, referred to as direct EM optimization in this study, is time-consuming and memory-intensive due to its need for massive EM simulations. In addition, direct EM optimization usually requires intensive engineers' experience to obtain a good initial design as input to the optimization subroutine. The quality of the final design obtained from direct EM optimization highly relies on the quality of the initial design. These issues become more intractable when the size of the metasurface becomes large and/or the metasurface's structural complexity becomes high.

To address the aforementioned issues, machine-learning (ML)-based approaches have been developed toward the goal of fast and intelligent metasurface design [4], [5], [6], [7], [8], [9], [10], [11], [12], [13], [14], [15], [16], [17]. However, most of the existing ML-based approaches to metasurface design are data-driven methods, which require a large amount of data to be generated by full-wave EM simulations. Subsequently, a surrogate model is developed through a training process by a certain ML technique. The adopted ML techniques include deep learning [4], [5], [6], [7], [8], [9],

Manuscript received 22 September 2022; revised 11 December 2022; accepted 15 January 2023. This work was supported in part by the Basic Scientific Center of Information Metamaterials of the National Natural Science Foundation of China under Grant 6228810001; in part by the National Key Research and Development Program of China under Grant 2017YFA0700201, Grant 2017YFA0700202, and Grant 2017YFA0700203; in part by the National Natural Science Foundation of China under Grant 62101124, Grant 62288101, Grant 62101382, and Grant 62271014; in part by the 111 Project under Grant 111-2-05; in part by the Major Project of Natural Science Foundation of Jiangsu Province under Grant BK20212002; and in part by the Natural Science Foundation of Jiangsu Province under Grant BK20210209 and Grant BK20220808. *(Corresponding authors: Jian Wei You; Tie Jun Cui.)*

Jianan Zhang, Jian Wei You, Zhuo Chen Lou, and Tie Jun Cui are with the State Key Laboratory of Millimeter Waves, Southeast University, Nanjing 210096, China (e-mail: jiananzhang@seu.edu.cn; jvyou@seu.edu.cn; 852588694@qq.com; tjcui@seu.edu.cn).

Feng Feng is with the School of Microelectronics, Tianjin University, Tianjin 300072, China (e-mail: ff@tju.edu.cn).

Weicong Na is with the Faculty of Information Technology, Beijing University of Technology, Beijing 100124, China (e-mail: weicongna@bjut.edu.cn).

Qi-Jun Zhang is with the Department of Electronics, Carleton University, Ottawa, ON K1S 5B6, Canada (e-mail: qjz@doe.carleton.ca).

Color versions of one or more figures in this article are available at https://doi.org/10.1109/TMTT.2023.3238076.

Digital Object Identifier 10.1109/TMTT.2023.3238076

kriging interpolation [10], [11], convolutional neural networks (CNNs) [12], [13], [14], and the Hopfield network [15]. These approaches suffer from a common issue, that is, as the structural complexity of the metasurface increases, the amount of data needed for the ML model development increases significantly. As a result, the computational burden for data generation by EM simulations becomes extremely high, and achieving an accurate data-driven surrogate model becomes quite difficult [18]. To alleviate this difficulty, physics-driven methods have been reported, which incorporate prior knowledge into the development of the surrogate model [16], [17]. In [16], a physics-driven ML technique has been reported for the design of meta-unit states for holographic imaging. The model combines the EM propagation model and generative adversarial network (GAN), which allows the reduction of training data while maintaining the model's physical interpretability. In [17], a prior-knowledge-guided synthesis method has been reported to optimize the performance of meta-cells with pixelated geometries. Fundamental EM theorems and experience have been utilized to reduce the amount of training data and the training time in developing the CNN-based surrogate model. Due to the incorporation of prior knowledge or physical principles into the model development process, physics-driven methods can, in general, achieve higher accuracy as well as better generality and physical interpretability than data-driven methods [19], [20].

Temporal coupled-mode theory (CMT) is a powerful tool in modeling multiresonator responses of optical/microwave systems [21], [22], [23], [24]. Recently, the possibility of utilizing CMT to guide the efficient inverse design of metasurfaces has been explored [25], [26]. In [25], CMT has been exploited to model the emission spectrum of a periodic array of coupled resonators. The correspondences between CMT parameters and geometrical design parameters have been stored in a lookup table (LUT), or called *catalog*, for single-resonator and double-resonator systems. Then, with these LUTs, the pattern search method has been used to achieve the inverse design of a multiresonator system with identical ribbons. The work in [25] has been extended to the design of far-field profiles of metasufaces in [26], where the constructed LUT has been combined with the adjoint optimization method to find the optimal metasuface design iteratively.

Both [25] and [26] require the LUTs as a premise to realize CMT-based metasurface design optimization. There are two major bottlenecks of these LUT-based CMT approaches in metasurface design. First, each item in the LUT contains one set of CMT parameter values and their corresponding geometrical parameter values. Each set of CMT parameter values is extracted from full-wave EM simulations of unit cells containing single- or double-resonators at the corresponding geometrical parameter value. As the dimension of the design parameter space increases, building the LUTs for practical parametric optimization would be extremely computationally expensive. Second, the constructed LUTs only contain the CMT parameters for a fixed group of geometrical parameter values. Metasurface design typically requires the optimization framework to search the design space iteratively to locate the optimal solution. In doing this, the design parameters repetitively change inside the parameter space and the EM responses of many new design parameter values have to be evaluated by EM solvers to optimize an objective function. Since the region of design space that covers the optimal metasurface design is typically unknown in advance, the size of the LUTs has to be dynamically increased during the optimization procedure, which significantly decreases the overall optimization efficiency.

To sum up, existing CMT methods have focused on the spectrum modeling of a coupled system with a fixed set of geometrical parameter values. To the best of our knowledge, the CMT has not been exploited to perform parametric modeling and expedite design optimization of metasurfaces, which is an indispensable part of the microwave CAD area. The application of the CMT approach to the parametric modeling of metasurfaces requires a systematic surrogate model development process with guaranteed high modeling accuracy, while applying CMT in expediting design optimization of metasurfaces calls for a novel optimization framework with suitable objective functions. Both aspects are investigated in this study.

In this article, we propose a novel physics-driven ML approach incorporating the CMT method for the efficient and intelligent design of metasurfaces. Our main contribution is the proposal of a novel surrogate-based method to facilitate the design optimization of multiresonator systems including metasurfaces, taking advantage of the CMT method. In the proposed approach, ML (in particular, the neural network technique) is combined with CMT to develop a surrogate model for fast prediction of EM responses of coupled multiresonator systems including metasurfaces. We name our proposed surrogate model as neuro-CMT model, which is developed in three stages. First, we perform full-wave EM simulations of unit cells only containing single- and double-resonators for different geometrical design parameter values. Second, we extract the single- and double-resonator CMT parameters for each geometrical parameter value by fitting the corresponding EM responses based on CMT equations. Third, we train neural networks to learn the relationships between the CMT parameters and geometrical parameters for single- and double-resonator systems, respectively. Once trained, the neural networks can provide fast and accurate predictions of the single- and double-resonator CMT parameters for new geometrical parameter values. These trained neural networks, in conjunction with the multiresonator CMT equation, become an efficient and physically interpretable tool to accurately predict the EM responses of any arbitrary coupled multiresonator systems. The proposed neuro-CMT model can be further utilized in fast and intelligent metasurface design optimizations.

II. Introduction to CMT-Based Modeling of Multiresonator Systems

In this section, we give a brief introduction to the CMT method, which has been widely used to model multiresonator systems, and establish some important notations to be used in Sections III–VI.

The microwave/optical system is comprised of multiple resonators in the form of a periodic array of coupled ribbons,

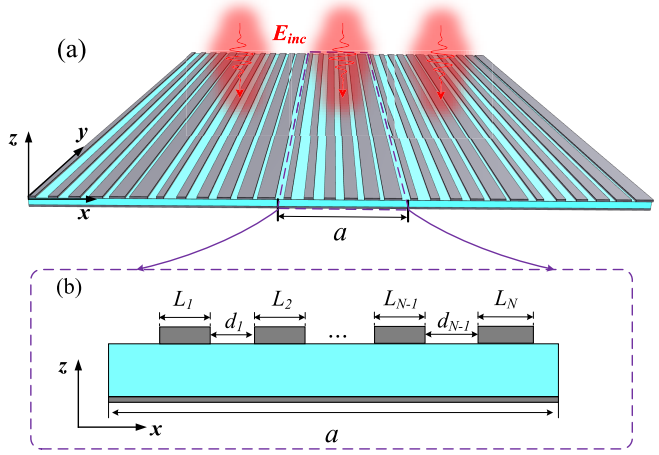

Fig. 1. (a) Schematic showing the periodic array of coupled ribbons. (b) Unit cell of the considered metasurface, where the periodical length is a and each unit contains several ribbons.

as shown in Fig. 1(a). Each unit cell of the periodic array consists of N coupled ribbons, as shown in Fig. 1(b). In general, such a system can be regarded as a set of N coupled resonances, described by the following CMT equations [21], [25]:

$$\frac{d\boldsymbol{a}}{dt} = j\boldsymbol{\Omega a} - \boldsymbol{\Gamma a} + \boldsymbol{D}s_+ \tag{1}$$

$$s_- = s_+ + \boldsymbol{D}^T\boldsymbol{a} \tag{2}$$

where $\boldsymbol{a} = [a_1, a_2, \ldots, a_N]^T$ represents the vector containing the mode amplitudes of the N resonances; s_+ and s_- represent the amplitude of the input wave and that of the output wave, respectively; $\boldsymbol{\Omega}$ is an $N \times N$ complex-valued matrix including the resonant frequencies and coupling constants between the resonators, expressed as [25]

$$\boldsymbol{\Omega} = \begin{bmatrix} \omega_0^1 & \beta_{12} & \cdots & \beta_{1N} \\ \beta_{21} & \omega_0^2 & \cdots & \beta_{2N} \\ \vdots & \vdots & \ddots & \vdots \\ \beta_{N1} & \beta_{N2} & \cdots & \omega_0^N \end{bmatrix} \tag{3}$$

where ω_0^i $(i = 1, 2, \ldots, N)$ represents the resonant frequency of resonator i. The symbol β_{ij} $(i, j = 1, 2, \ldots, N)$ represents the coupling constant between resonator i and resonator j, and we assume that $\beta_{ij} = \beta_{ji}$. The symbol $\boldsymbol{\Gamma}$ in (1) represents a real-valued $N \times N$ matrix containing the decay rates of the resonators, expressed as [25]

$$\boldsymbol{\Gamma} = \begin{bmatrix} \gamma_{a1} + \gamma_{r1} & \sqrt{\gamma_{r1}\gamma_{r2}} & \cdots & \sqrt{\gamma_{r1}\gamma_{rN}} \\ \sqrt{\gamma_{r2}\gamma_{r1}} & \gamma_{a2} + \gamma_{r2} & \cdots & \sqrt{\gamma_{r2}\gamma_{rN}} \\ \vdots & \vdots & \ddots & \vdots \\ \sqrt{\gamma_{rN}\gamma_{r1}} & \sqrt{\gamma_{rN}\gamma_{r2}} & \cdots & \gamma_{aN} + \gamma_{rN} \end{bmatrix} \tag{4}$$

where γ_{ai} and γ_{ri} $(i = 1, 2, \ldots, N)$ represent the absorptive decay rate and radiative decay rate of resonator i, respectively. The symbol $\boldsymbol{D}$ is a complex-valued $N \times 1$ vector, which allows the system to be coupled to the incoming and outgoing plane waves, given by [25]

$$\boldsymbol{D} = j[\sqrt{2\gamma_{r1}} \quad \sqrt{2\gamma_{r2}} \quad \cdots \quad \sqrt{2\gamma_{rN}}]^T. \tag{5}$$

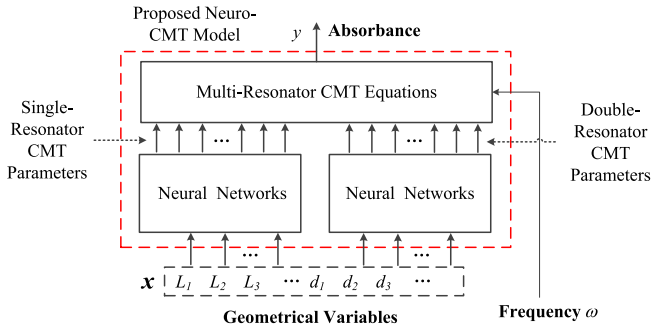

Fig. 2. Structure of the proposed neuro-CMT model.

Let $\alpha(\omega)$ represent the absorbance of the system at frequency ω. Due to the presence of a perfect electric conductor (PEC) background, the system under consideration does not have any transmission, and the absorbance is calculated as 1 − reflectivity. Based on (1) and (2), one can derive the absorbance of the system as follows [25]:

$$\alpha(\omega) = 1 - |1 + \boldsymbol{D}^T(j(\omega\boldsymbol{I}_N - \boldsymbol{\Omega}) + \boldsymbol{\Gamma})^{-1}\boldsymbol{D}|^2 \tag{6}$$

where $\boldsymbol{I}_N$ represents the $N \times N$ identity matrix.

One crucial step in CMT-based modeling of multiresonator systems is to extract the CMT parameters (i.e., ω_0^i, γ_{ai}, γ_{ri}, and β_{ij}) of single- and double-resonator systems from full-wave EM simulations. This can be done by first fitting the single-resonator EM simulation data with the following equation [25]:

$$\alpha(\omega) = \frac{4\gamma_a\gamma_r}{(\omega - \omega_0)^2 + (\gamma_a + \gamma_r)^2} \tag{7}$$

which is derived from (6) with letting $N = 1$. Fitting (7) to the EM simulation data gives one the values of ω_0, γ_a, and γ_r. Then, the double-resonator CMT parameters can be extracted in a similar way, by fitting the EM data with the CMT equation (6) with $N = 2$. Based on the extracted CMT parameters, one can achieve accurate predictions of the EM responses (e.g., absorbance) of a coupled N-resonator (here each ribbon plays as one resonator) system, as long as the resonant frequency and decay rates of every single ribbon and the coupling constant for each pair of ribbons have been extracted in advance.

The above existing CMT-based approach focuses on the spectrum modeling of a coupled system at a fixed set of geometrical parameter values. Practical metasurface design usually exploits an optimization framework in which the geometrical parameters are repetitively updated to locate the optimal solution in the design parameter space. During this procedure, the optimizer drives EM solvers to evaluate the EM responses of many new sets of geometrical parameter values, to achieve the minimization of a certain objective function. As a result, the existing CMT-based modeling approach has to repetitively reextract the single- and double-resonator CMT parameters from EM simulations, which significantly deteriorates the overall optimization efficiency. In Section III, we propose a novel physics-driven ML approach incorporating CMT, named the neuro-CMT approach, to address this issue.

III. Proposed Neuro-CMT Modeling of Multiresonator Systems

The structure of the proposed neuro-CMT model is shown in Fig. 2. The model has three main components, that is, neural networks for single-resonator CMT parameters, neural networks for double-resonator CMT parameters, and multiresonantor CMT equations. The input parameters in our proposed model are design variables (i.e., geometrical parameters) of the multiresonator system (i.e., metasurface) as well as frequency. The output of the model, denoted by y, is the EM response (e.g., absorbance) of the metasurface. Let $\boldsymbol{x}$ denote the vector of design variables for the metasurface under consideration. For the unit cell shown in Fig. 1(b), we consider that the design parameters contain the lengths of all the ribbons and the distances between two neighboring ribbons, that is, $\boldsymbol{x} = [L_1, L_2, \ldots, L_N, d_1, d_2, \ldots, d_{N-1}]^T$. For notational convenience in subsequent descriptions, we express $\boldsymbol{x}$ as $\boldsymbol{x} = [x_1, x_2, \ldots, x_k, \ldots, x_K]^T$, where $K = 2N - 1$ and x_k denotes the kth element in $\boldsymbol{x}$.

As geometrical parameters $\boldsymbol{x}$ change, the CMT parameters ω_i, γ_{ai}, γ_{ri}, and β_{ij} change accordingly. In the existing CMT-based approaches [25], [26], as geometrical parameters change to a new value in a certain optimization framework, the single- and double-ribbon CMT fitting processes have to be reexecuted to extract a new set of CMT parameters. However, two issues arise as one reextracts the new set of CMT parameters. First, the time-consuming nature of full-wave EM simulations makes the one-time extraction of the CMT parameters computationally expensive. Second, EM optimization usually requires repetitive changes of the geometrical parameter values, which necessitates massive extractions of the CMT parameters. To achieve fast and accurate predictions of CMT parameters as geometrical parameters change, we propose to train two neural networks (one for a single-resonator system and the other one for a double-resonator system) to learn the relationships between the CMT parameters and the geometrical parameters.

A. Neural Network Model Development for Single-Resonator CMT Parameters Prediction

The development of the neural network model for single-resonator CMT parameters prediction mainly contains the following two steps.

1) Extraction of the Data of Single-Resonator Parameters: The structure of a unit cell containing only one ribbon is shown in Fig. 3(a). Let L represent the length of the ribbon along the x-axis. As L changes, the CMT parameters ω_0, γ_a, and γ_r change accordingly. Our aim is to develop a neural network model to achieve fast and accurate predictions of the three CMT parameters for a given L. The input to the model is L, while the outputs of the model are ω_0, γ_a, and γ_r.

The development process begins with the generation of training data by performing full-wave EM simulations of unit cells containing single resonators with different L values. Let M_1 be the number of training samples for the single-resonator neural network. Let $\mathcal{I}_1$ represent the index set of the training samples at different values of L, that is, $\mathcal{I}_1 = \{1, 2, \ldots, M_1\}$. Let $L^{(n)}$ represent the nth ($n \in \mathcal{I}_1$) geometrical sample in the training data.

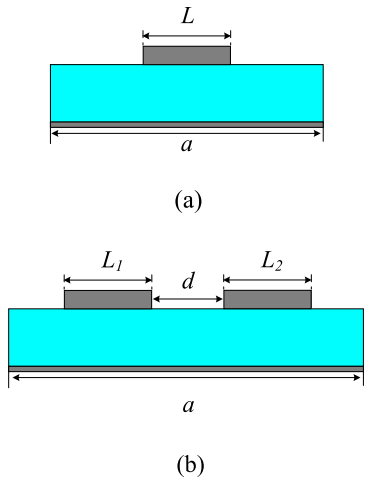

Fig. 3. (a) Unit cell structure containing one ribbon. (b) Unit cell structure containing two ribbons.

For each geometrical parameter value $L^{(n)}$, ($n \in \mathcal{I}_1$), we perform full-wave EM simulations to obtain the EM response (i.e., absorbance) of the corresponding metasurface. Let ω_f represent the fth frequency sample of interest, where $f \in \mathcal{F}$ and $\mathcal{F}$ is a set containing all the frequency samples of interest. Let $\alpha^{(n)}(\omega_f)$ represent the absorbance at $L^{(n)}$ and ω_f. The resonant frequency $\omega_0^{(n)}$ corresponding to $L^{(n)}$ is extracted by finding the peak of the EM response curve, while the decay rates γ_a and γ_r corresponding to $L^{(n)}$ are extracted by performing the following 2-D unconstrained minimization:

$$\left\{\gamma_a^{(n)}, \gamma_r^{(n)}\right\} = \arg\min_{\gamma_a, \gamma_r} \sum_{f \in \mathcal{F}} \left(\left| \frac{4\gamma_a \gamma_r}{(\omega_f - \omega_0)^2 + (\gamma_a + \gamma_r)^2} \right| - |\alpha^{(n)}(\omega_f)| \right)^2 \tag{8}$$

where $|\cdot|$ represents the magnitude of a number. One can note that the problem in (8) is a nonlinear unconstrained optimization problem. It can be solved by classical numerical methods and we adopt the Nelder–Mead simplex direct search algorithm [27] implemented in MATLAB in this study.

2) Single-Resonant Neural Network Training: The above procedure generates one training sample $\{L^{(n)}, \boldsymbol{d}^{(n)}\}$, where $\boldsymbol{d}^{(n)} = [\omega_0^{(n)}, \gamma_a^{(n)}, \gamma_r^{(n)}]^T$. Once the training dataset has been obtained for all the geometrical parameter values, we use a three-layer multilayer perception (MLP) neural network to learn the relationship between the CMT parameters and the geometrical parameter L.

Let the output vector of the single-resonator neural network be denoted as $\boldsymbol{y}_{\text{sr}} = [\bar{\omega}_0, \bar{\gamma}_a, \bar{\gamma}_r]^T$. Let $\boldsymbol{w}_{\text{sr}}$ represent the single-resonator neural network weights. The training process can be formulated as the following optimization problem:

$$\boldsymbol{w}_{\text{sr}}^* = \arg\min_{\boldsymbol{w}_{\text{sr}}} E_1(\boldsymbol{w}_{\text{sr}}) \tag{9}$$

where $E_1(\boldsymbol{w}_{\text{sr}})$ is the training error function for the single-resonator neural network, defined as

$$E_1(\boldsymbol{w}_{\text{sr}}) = \frac{1}{2M_1} \sum_{n \in \mathcal{I}_1} \|\boldsymbol{y}_{\text{sr}}(L^{(n)}, \boldsymbol{w}_{\text{sr}}) - \boldsymbol{d}^{(n)}\|^2. \tag{10}$$

The purpose of the above training process is to minimize the differences between the neural network outputs and the

data of the three CMT parameters extracted from the EM responses. By doing this, fast and accurate predictions of the single-ribbon CMT parameters can be provided by the trained neural network for a new value of L.

B. Neural Network Model Development for Double-Resonant CMT Parameter Prediction

The development of the neural network model for double-resonator CMT parameters contains the following two steps.

1) Extraction of the Data of Double-Resonator Parameters: The structure of a unit cell containing two ribbons is illustrated in Fig. 3(b). Let L_1 and L_2 represent the lengths of the two ribbons along the x-axis. Let d denote the distance between the two ribbons. As the three geometrical parameters (i.e., L_1, L_2, and d) change, the coupling constant β_{12} changes accordingly. Our aim is to develop a neural network model to achieve fast yet accurate predictions of the CMT parameter β_{12} for a given geometrical parameter combination (i.e., geometrical sample) $\{L_1, L_2, d\}$. Define the vector of geometrical parameters as $\boldsymbol{z} = [L_1 \ L_2 \ d]^T$. The inputs to the model are $\boldsymbol{z}$, while the outputs of the model are the real and imaginary parts of β_{12}.

We start with training data generation by performing full-wave EM simulations of unit cells containing double resonators with different geometrical samples. Let M_2 be the number of training samples for the double-resonator neural network. Let $\mathcal{I}_2$ represent the index set of the training samples at different geometrical samples, that is, $\mathcal{I}_2 = \{1, 2, \ldots, M_2\}$. Let $\boldsymbol{z}^{(m)}$ represent the mth ($m \in \mathcal{I}_2$) geometrical sample in the training data, where $\boldsymbol{z}^{(m)} = [L_1^{(m)} \ L_2^{(m)} \ d^{(m)}]^T$.

For each geometrical sample $\boldsymbol{z}^{(m)}$, we perform full-wave EM simulations to obtain the EM response (i.e., absorbance) of the corresponding metasurface. Let $\alpha^{(m)}(\omega_f)$ represent the absorbance at $\boldsymbol{z}^{(m)}$ and ω_f. The real and imaginary parts of the coupling constant corresponding to $\boldsymbol{z}^{(m)}$ are extracted by performing the following unconstrained minimization:

$$\beta_{12}^* = \arg\min_{\beta_{12}} \sum_{f\in\mathcal{F}} (|\alpha(\beta_{12}, \omega_f)| - |\alpha^{(m)}(\omega_f)|)^2 \tag{11}$$

where the explicit expression of $\alpha(\beta_{12}, \omega_f)$ is given by (6) with letting $N = 2$. Note that in the above minimization problem, the single-resonator CMT parameters for the two ribbons should be available already, leaving the coupling constant β_{12} as the only free variable. With the single-resonator CMT parameters extracted for L_1 and L_2 being available, the nonlinear unconstrained optimization problem in (11) is solved by the Nelder–Mead simplex direct search algorithm [27].

2) Double-Resonant Neural Network Training: The aforementioned procedure generates one training sample $\{\boldsymbol{z}^{(m)}, \boldsymbol{c}^{(m)}\}$, where $\boldsymbol{c}^{(m)} = [\mathrm{Re}(\beta_{12})^{(m)} \ \mathrm{Im}(\beta_{12})^{(m)}]^T$. Once the training dataset has been obtained for all the geometrical samples, we use a three-layer MLP to learn the relationship between the CMT parameters and the three geometrical parameters contained in $\boldsymbol{z}$.

Let the output vector of the neural network be denoted as $\boldsymbol{y}_{\mathrm{dr}} = [\mathrm{Re}(\bar{\beta}_{12}) \ \mathrm{Im}(\bar{\beta}_{12})]^T$. Let $\boldsymbol{w}_{\mathrm{dr}}$ represent the double-resonator neural network weights. The training process

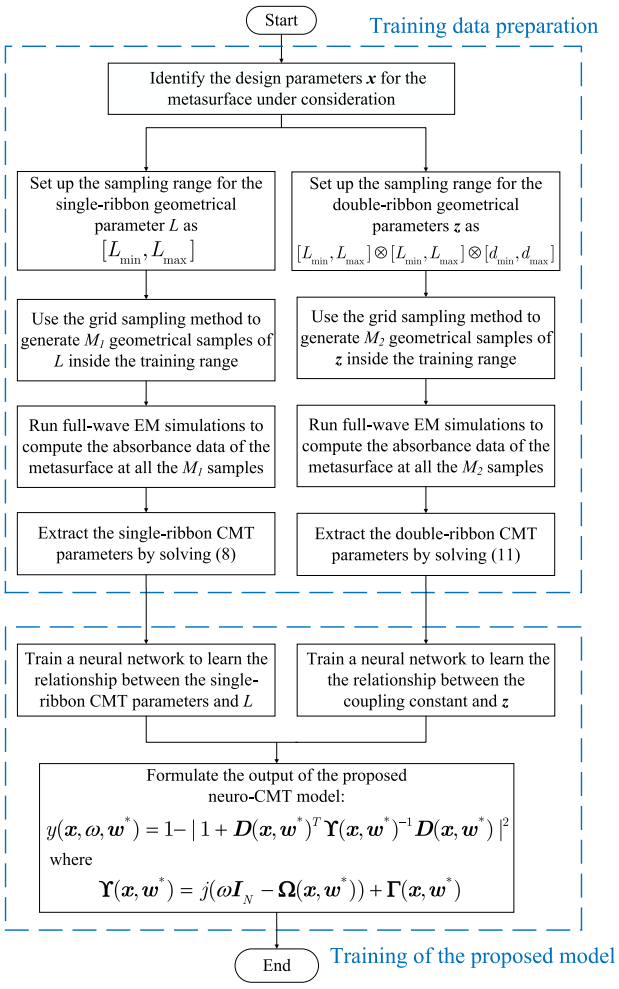

Fig. 4. Flowchart for developing the proposed neuro-CMT model.

can be formulated as the following optimization problem:

$$\boldsymbol{w}_{\mathrm{dr}}^* = \arg\min_{\boldsymbol{w}_{\mathrm{dr}}} E_2(\boldsymbol{w}_{\mathrm{dr}}) \tag{12}$$

where $E_2(\boldsymbol{w}_{\mathrm{dr}})$ is the training error function for the double-resonator neural network, defined as

$$E_2(\boldsymbol{w}_{\mathrm{dr}}) = \frac{1}{2M_2} \sum_{m\in\mathcal{I}_2} \|\boldsymbol{y}_{\mathrm{dr}}(\boldsymbol{z}^{(m)}, \boldsymbol{w}_{\mathrm{dr}}) - \boldsymbol{c}^{(m)}\|^2. \tag{13}$$

Once the training process in (12) is done, the trained neural network can provide fast and accurate predictions of the coupling constant for any new combination of geometrical parameter values $\{L_1, L_2, d\}$.

The two trained neural networks along with the multiresonator CMT equations (3)–(6) form the proposed CMT model, as shown in Fig. 2. Let $\boldsymbol{w}^*$ be the vector of the optimized neural network weights for the two neural networks, that is, $\boldsymbol{w}^* = [(\boldsymbol{w}_{\mathrm{sr}}^*)^T \ (\boldsymbol{w}_{\mathrm{dr}}^*)^T]^T$. Then, the output of the neuro-CMT model is given by

$$y(\boldsymbol{x}, \omega, \boldsymbol{w}^*) = 1 - |1 + \boldsymbol{D}(\boldsymbol{x}, \boldsymbol{w}^*)^T \boldsymbol{\Upsilon}^{-1}(\boldsymbol{x}, \boldsymbol{w}^*) \boldsymbol{D}(\boldsymbol{x}, \boldsymbol{w}^*)|^2 \tag{14}$$

where $\boldsymbol{\Upsilon}(\boldsymbol{x}, \boldsymbol{w}^*)$ is an $N \times N$ complex-valued matrix, defined as

$$\boldsymbol{\Upsilon}(\boldsymbol{x}, \boldsymbol{w}^*) = j(\omega \boldsymbol{I}_N - \boldsymbol{\Omega}(\boldsymbol{x}, \boldsymbol{w}^*)) + \boldsymbol{\Gamma}(\boldsymbol{x}, \boldsymbol{w}^*). \tag{15}$$

Equation (14) allows us to predict the EM responses of a coupled, N-resonant system at any geometrical parameter value $\boldsymbol{x}$ efficiently and accurately, as demonstrated in Section VI.

C. Stepwise Algorithm for Developing the Proposed Neuro-CMT Model

The flowchart of developing the proposed neuro-CMT model is shown in Fig. 4. The development process can also be summarized into the following stepwise algorithm.

- *Step 1):* Set up the sampling range for the single-ribbon geometrical parameter L as $[L_{\min}, L_{\max}]$.
- *Step 2):* Use the grid sampling method to generate M_1 geometrical samples inside the training range $[L_{\min}, L_{\max}]$, that is, $\{L^{(1)}, L^{(2)}, \ldots, L^{(n)}, \ldots, L^{(M_1)}\}$.
- *Step 3):* For each geometrical value $L^{(n)}$, $n \in \mathcal{I}_1$, perform full-wave EM simulations to compute the absorbance of the metasurface corresponding to $L^{(n)}$.
- *Step 4):* Extract the single-ribbon CMT parameters $\{\gamma_a^{(n)}, \gamma_r^{(n)}\}$ by solving the optimization (8) with classical numerical methods (i.e., the Nelder–Mead simplex direct search algorithm), for $n = 1, 2, \ldots, M_1$.
- *Step 5):* Train an MLP to learn the relationship between the single-ribbon CMT parameters and geometrical parameter L based on (9) and (10).
- *Step 6):* For the double-ribbon case, denote the sampling ranges of the three parameters as $[L_{\min}, L_{\max}]$, $[L_{\min}, L_{\max}]$, and $[d_{\min}, d_{\max}]$, respectively. Use the grid sampling method to generate M_2 geometrical samples inside the 3-D parameter space, that is, $\{\boldsymbol{z}^{(1)}, \boldsymbol{z}^{(2)}, \ldots, \boldsymbol{z}^{(M_2)}\}$.
- *Step 7):* For each geometrical sample $\boldsymbol{z}^{(m)}$, $m \in \mathcal{I}_2$, perform full-wave EM simulations to compute the absorbance of the metasurface corresponding to $\boldsymbol{z}^{(m)}$.
- *Step 8):* Extract the double-ribbon CMT parameters $\{\mathrm{Re}(\beta_{12}^{(m)}), \mathrm{Im}(\beta_{12}^{(m)})\}$ by solving the optimization (11) with the Nelder–Mead simplex direct search algorithm, for $m = 1, 2, \ldots, M_2$.
- *Step 9):* Train an MLP to learn the relationship between the double-ribbon CMT parameters and the three geometrical parameters $\{L_1, L_2, d\}$ based on (12).
- *Step 10):* Formulate the output of the proposed neuro-CMT model as shown in (14) and (15).
- *Step 11):* The model development process terminates.

By incorporating the CMT equations into the model structure, the neuro-CMT model developed by the above procedure has much better physical interpretability than that of the data-driven method. Besides, another important advantage of the proposed approach over the data-driven method and many other existing parametric modeling methods (such as [28] and [29]) is that it allows "multipurpose use" with only "one-time training." This means that once the training of the single- and double-resonator neural networks is done, the resultant neuro-CMT model allows fast and accurate prediction of the EM response of coupled systems with any number of resonators. Assuming that the size of the unit cell does not change, the model can be further utilized in metasurface design optimizations with different functional purposes, without the need of developing a new parametric model from scratch. We demonstrate this advantage of the proposed approach in Section VI.

IV. Neuro-CMT-Assisted Design Optimization of Metasurfaces

The proposed neuro-CMT model developed in Section III can be further utilized to achieve rapid design optimizations of metasurfaces, in which the geometrical parameters $\boldsymbol{x}$ are considered as the optimization variables. The design of a metasurface with unit cell shown in Fig. 1(b) can be formulated as the following constrained optimization:

$$\begin{aligned} \boldsymbol{x}^* = \arg\min_{\boldsymbol{x}} \; & U(\boldsymbol{x}) \\ \text{s.t. } & x_k \in [L_{\min}, L_{\max}] \quad \forall k = 1, 2, \ldots, N \\ & x_k \in [d_{\min}, d_{\max}] \quad \forall k = N+1, \ldots, 2N-1 \\ & \sum_{k=1}^{K} x_k \le a \end{aligned} \tag{16}$$

where a is the length of the unit cell along the x-axis, and $U(\cdot)$ represents either a minimax or generalized l_p error function [30]. For example, for a frequency-selected or wideband microwave absorber considered in this study, the objective function of optimization takes the following form:

$$U(\boldsymbol{x}) = \sum_{f \in \mathcal{F}} e(\boldsymbol{x}, \omega_f) \tag{17}$$

where $\mathcal{F}$ represents the set containing the indices of all the frequency samples at which a design specification sample exists; $e(\boldsymbol{x}, \omega_f)$ is computed from

$$e(\boldsymbol{x}, \omega_f) = \begin{cases} y(\boldsymbol{x}, \omega_f) - S(\omega_f), & \text{if } S(\omega_f) \in \mathcal{S}_u \\ S(\omega_f) - y(\boldsymbol{x}, \omega_f), & \text{if } S(\omega_f) \in \mathcal{S}_l \end{cases} \tag{18}$$

where $S(\omega_f)$ represents the design specification imposed on frequency ω_f, and $\mathcal{S}_u$ and $\mathcal{S}_l$ are two sets that contain all the upper and the lower design specification samples for the absorber, respectively. In this study, $\boldsymbol{x}^*$ is found by solving (16) using the quasi-Newton method.

We emphasize that the replacement of a full-wave EM solver by the proposed neuro-CMT model allows one to avoid the massive EM simulations in metasurface design optimization. With the ability of fast and accurate predictions of the EM responses of the metasurface subject to varying geometrical parameters, the proposed neuro-CMT approach can facilitate the design of metasurfaces significantly.

V. Discussion

The two neuro-CMT-based design optimization examples presented in this study consider microwave absorbers whose unit cells contain three ($N = 3$) and six ($N = 6$) coupled ribbons, respectively. This results in the number of inputs to the proposed neuro-CMT model being five ($K = 5$) and 11 ($K = 11$), respectively. Theoretically, the proposed approach

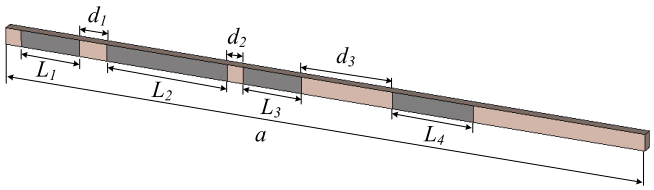

Fig. 5. EM structure of the unit cell (with $N = 4$ ribbons) of the microwave absorber to be used to evaluate the modeling performance of the neuro-CMT approach.

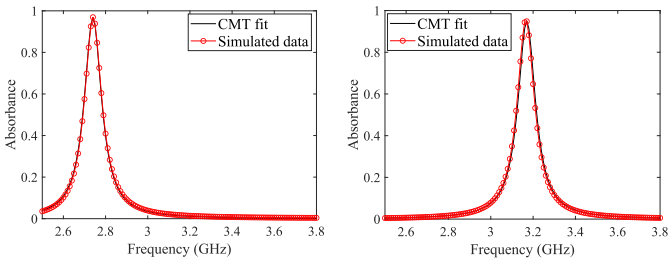

Fig. 6. Extraction of single-resonator CMT parameters and the fitting results between the CMT equation and the CST simulated data. (a) Fitting results for $L = 22$ (mm). (b) Fitting results for $L = 18$ (mm).

is directly applicable to higher dimensional cases (i.e., unit cells with more coupled ribbons), upon the size of the unit cell a and the material properties of the substrate being fixed. However, the performance of CMT in modeling multiresonator systems may degrade as N increases, leading to an accuracy loss of the proposed neuro-CMT model. We leave how to improve the CMT prediction accuracy in high-dimensional cases as a future research direction.

Theoretically, the proposed neuro-CMT approach is universal and can deal with 1-D and 2-D periodic structures (metasurfaces) with various optimization objectives [24], [26]. In this article, we use a 1-D periodic array of coupled ribbons with linear polarization and vertical incident waves to more clearly demonstrate the numerical implementation and effectiveness of the proposed approach. For other types of metasurfaces and/or more difficult design objectives (such as wideband absorbers with other polarization or angles of incident waves), the proposed approach is still applicable provided that sufficient training data can be acquired by performing corresponding EM simulations.

We set periodical boundary conditions when performing full-wave EM simulations of single and double resonators. By increasing the number of periodic cells in fabrication or compensating the EM model to take into consideration the edge truncation effect, we can develop a training database as accurate as that measured in practical experiments. Once the training database is accurate, our proposed neuro-CMT model output will remain to be correct and accurate.

VI. Application Examples

A. Parametric Modeling of a Microwave Absorber With Multiple PEC Ribbons

To evaluate the modeling performance of the proposed neuro-CMT approach, we perform parametric modeling of a microwave absorber, whose unit cell (with $N = 4$ ribbons as an example) is shown in Fig. 5. The length of the unit cell along the x-axis is $a = 200$ (mm), while the height along the z-axis is 3 mm. A lossy FR-4 substrate with a thickness of 3 mm, dielectric constant $\varepsilon_r = 4.3$, and loss tangent $\delta = 0.025$ is used for the metasurface-based absorber. The absorber is periodic along both the x- and y-axes. We next evaluate the performance of the proposed neuro-CMT approach in parametric modeling of the microwave absorber with different numbers of ribbons in each unit cell.

For single-ribbon CMT parameter extractions, we set the sampling range as $[L_{\min}, L_{\max}] = [13, 30]$ (mm) and the number of geometrical samples as $M_1 = 171$. The frequency-domain solver (i.e., the finite-element method) in the CST software is used to perform EM simulations to obtain the data of the absorbance at the frequency range of interest (i.e., 2–4 GHz). The absorbance is calculated for a normally incident TM-polarized (H-field in the y-direction) plane wave. Each simulation takes about 2 min 20 s to complete on an AMD Ryzen Threadripper 3960X 24-Core Processor @3.79 GHz. After the generation of the EM simulation data is done, we use the "fminsearch" function in MATLAB (which is an example implementation of the Nelder–Mead direct search algorithm) to fit the response curve for each value of L in the 171 samples. Fig. 6(a) and (b) shows the fitting results for $L = 22$ (mm) and $L = 18$ (mm), respectively. We can see from Fig. 6(a) and (b) that, with the optimized values of the CMT parameters, the single-resonator responses predicted by the CMT equation [see (7)] agree very well with the EM data. The CMT parameters extracted from these fitting processes for $L = 22$ (mm) are $\omega_0 = 1.7216 \times 10^{10}$ (rad/s), $\gamma_a = 1.8493 \times 10^8$ (rad/s), and $\gamma_r = 1.2915 \times 10^8$ (rad/s), and those for $L = 18$ (mm) are $\omega_0 = 1.9918 \times 10^{10}$ (rad/s), $\gamma_a = 1.927 \times 10^8$ (rad/s), and $\gamma_r = 1.2243 \times 10^8$ (rad/s).

For double-ribbon CMT parameter extractions, we set $d_{\min} = 1$ (mm) and $d_{\max} = 171$ (mm). The sampling spaces for the three geometrical parameters (i.e., L_1, L_2, and d) are 1, 1, and 5 mm, respectively. This results in a total of $18 \times 18 \times 35 = 11\,340$ geometrical samples in the design parameter space. Note that such a sampling scheme guarantees that the coupling coefficient predicted by the double-resonator neural network covers all possible parameter combinations within the unit cell's size. Due to the periodicity of the ribbon array, the coupling constant is mirror-symmetric about $d = (a - (L_1 + L_2))/2$ [25]. Therefore, nearly half of the geometrical samples can be omitted in the EM simulation and CMT parameter extraction processes. After removing the redundant samples, the total number of geometrical samples in the double-resonator CMT parameter extraction process turns out to be $M_2 = 5200$. Each simulation of the double-ribbon system takes about 2.5 min to finish. A cluster of computers is employed to evaluate the EM responses at the 5200 geometrical samples in parallel. The total time for training data acquisition of the proposed neuro-CMT model is about 10 h.

Once the generation of the EM simulation data for the double-resonator system at all the geometrical samples is done, the Nelder–Mead direct search algorithm is employed to fit the absorbance response curve based on (11) for each of the 5200 samples. Fig. 7(a)–(d) shows the fitting results at four

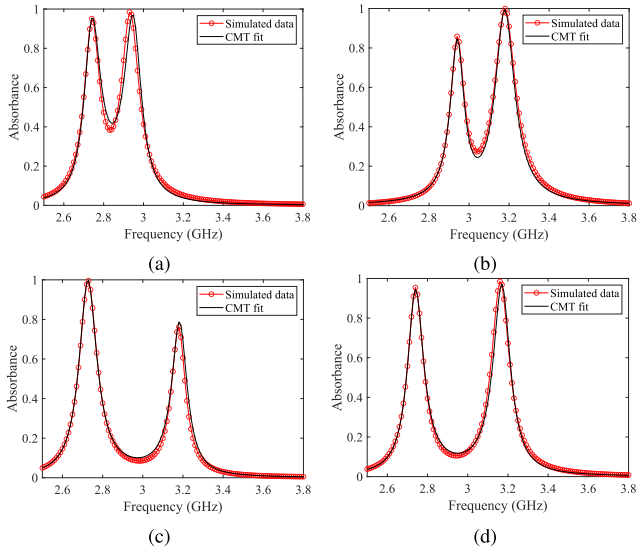

Fig. 7. Extraction of double-resonator CMT parameters and the fitting results between the responses predicted by the CMT equation and the CST simulated data. (a) Fitting results at $[L_1\ L_2\ d] = [20\ 22\ 20]$ (mm). (b) Fitting results at $[L_1\ L_2\ d] = [20\ 18\ 47]$ (mm). (c) Fitting results at $[L_1\ L_2\ d] = [22\ 18\ 5]$ (mm). (d) Fitting results at $[L_1\ L_2\ d] = [22\ 18\ 28]$ (mm).

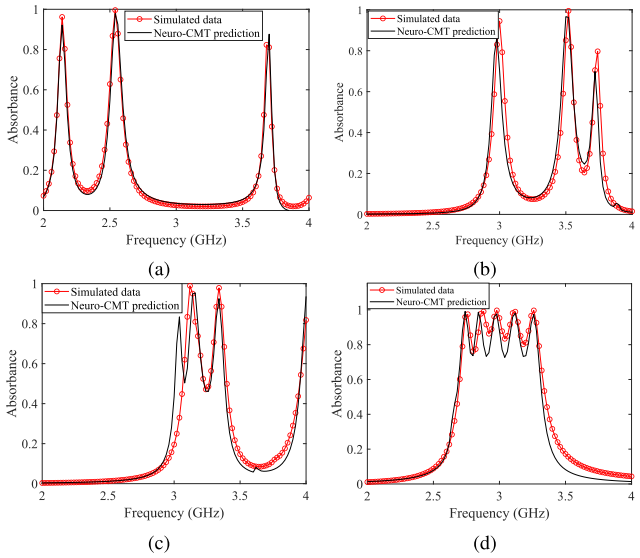

Fig. 8. Comparison between the neuro-CMT predictions and the CST simulated data at four selected geometrical samples for multiribbon cases. (a) $N = 3$. (b) $N = 4$. (c) $N = 5$. (d) $N = 6$. Note that these predictions cannot be done by the MLP3 and the neuro-TF models merely trained with the EM data corresponding to $N = 2$.

TABLE I

DOUBLE-RESONANCE CMT PARAMETER EXTRACTION RESULTS FOR THE FOUR SELECTED GEOMETRICAL SAMPLES

L_1 (mm)	L_2 (mm)	d (mm)	Re(β_{12}) (rad/s)	Im(β_{12}) (rad/s)
20	22	20	3.1748e+07	-5.6136e+07
22	18	47	2.9584e+08	1.8032e+07
22	18	5	-5.0764e+08	-5.7990e+07
22	18	28	1.2919e+08	-4.5322e+07

selected geometrical samples for illustration purposes. One can observe from Fig. 7(a)–(d) that, with the optimized values of the coupling constant, the absorbance predicted by the CMT equation agrees remarkably well with the EM data. The CMT parameters extracted from these fitting processes for the four selected geometrical samples are listed in Table I.

Given the extracted data of CMT parameters, we next train two three-layer MLPs to learn the relationship between the CMT parameters and the geometrical parameter(s). The number of hidden neurons for the single-resonator neural network and that for the double-resonator neural network are 5 and 20, respectively. The neural network training and model output formulation are implemented in the *Neuro-ModelerPlus* software [31]. The training time of the single- and double-resonator neural networks are about 5 and 25 s, respectively.

Once the single- and double-resonator neural networks are trained, they can be reused to build the parametric model for the metasurface with different numbers of resonators in each unit cell. To demonstrate this advantage and verify the modeling accuracy of the proposed neuro-CMT model, we compare the model output with EM data at several geometrical samples. Fig. 8 compares the neuro-CMT prediction with the corresponding EM data. This comparison is done at four different test geometrical parameter values corresponding to four different numbers of resonators in each unit cell.

1) *Test Geometrical Parameter Value #1 ($N = 3$):* $\boldsymbol{x} = [13.5\ 29.5\ 24.1667\ 29.6667\ 83.0]^T$ (mm).
2) *Test Geometrical Parameter Value #2 ($N = 4$):* $\boldsymbol{x} = [19.5\ 13.5\ 13.5\ 13.5\ 13.0\ 3.0\ 13.0]^T$ (mm).
3) *Test Geometrical Parameter Value #3 ($N = 5$):* $\boldsymbol{x} = [13\ 17.88\ 18.05\ 16.84\ 13.0\ 10\ 10\ 14.53\ 10.0]^T$ (mm).
4) *Test Geometrical Parameter Value #4 ($N = 6$):* $\boldsymbol{x} = [18.84\ 22.02\ 19.71\ 17.57\ 22.43\ 20.76\ 6.07\ 5\ 6.81\ 16.71\ 30]^T$ (mm).

Note that for all of the four test samples above, their data of single- and double-resonator CMT parameters have not been used in the two neural network training processes. But clearly one can observe from Fig. 8 that the neuro-CMT predictions match the EM data well for all the four selected test geometrical samples.

For comparison purposes, we first apply the data-driven approach (i.e., the three-layer perception, MLP3) and the neuro-TF method [28] to perform parametric modeling of the absorber with two ribbons existing in each unit cell ($N = 2$). Two different cases of geometrical parameter ranges are considered. Table II shows the definitions of training and testing data for the three methods in comparison. In Case 1, the geometrical parameters change in a smaller range, while in Case 2, the geometrical parameters change in a wider range. Table III compares the modeling performance among the three methods (the number of hidden neurons for all three methods are tuned to be optimal). In Case 1, all methods achieve a very small and comparable testing error. In Case 2, with the same amount of training data, the proposed method achieves the smallest training and testing errors among the three methods. Fig. 9 compares the modeling results for the three methods at two selected geometrical samples in Case 2 for $N = 2$.

Additionally, one remarkable advantage of the proposed approach is that the neural networks developed for $N = 2$ in

TABLE II

DEFINITION OF TRAINING AND TESTING DATA FOR THE PARAMETRIC MODELING OF THE MICROWAVE ABSORBER

Geometrical Variables		Training Data			Testing Data		
		Min	Max	Step	Min	Max	Step
Case 1 ($N = 2$)	L_1 (mm)	16	18	0.2	16.1	17.9	0.2
	L_2 (mm)	16	18	0.2	16.1	17.9	0.2
	d_1 (mm)	10	0.2	11	10.1	0.2	10.9
Case 2 ($N = 2$)	L_1 (mm)	13	30	1.0	13.5	29.5	1.0
	L_2 (mm)	13	30	1.0	13.5	29.5	1.0
	d_1 (mm)	1	171	5.0	3	168	5.0
Case 3 ($N = 3$)	L_1 (mm)	13	30	2.83	14.5	28.5	4.67
	L_2 (mm)	13	30	2.83	14.5	28.5	4.67
	L_3 (mm)	13	30	2.83	14.5	28.5	4.67
	d_1 (mm)	1	171	28.33	15	167	50.67
	d_2 (mm)	1	171	28.33	15	167	50.67

TABLE III

MODELING PERFORMANCE COMPARISONS OF THE THREE MODELING METHODS FOR THE MICROWAVE ABSORBER

Modeling Method		# of Hidden Neurons	# of Training Samples	Average Training Error	Average Testing Error
Case 1 (N=2)	Data-driven (MLP3)	30	726	0.78%	0.72%
	neuro-TF	10 + 10	726	0.75%	0.65%
	neuro-CMT (Proposed)	5 + 15	726	0.68%	0.63%
Case 2 (N=2)	Data-driven (MLP3)	50	5200	7.84%	7.62%
	neuro-TF	15 + 15	5200	5.48%	4.63%
	neuro-CMT (Proposed)	5 + 20	5200	4.82%	4.32%
Case 3 (N=3)	Data-driven (MLP3)	50	5629	14.39%	16.79%
	neuro-TF	20 + 20	5629	21.35%	22.39%
	neuro-CMT (Proposed)	5 + 20	0	N/A	5.31%

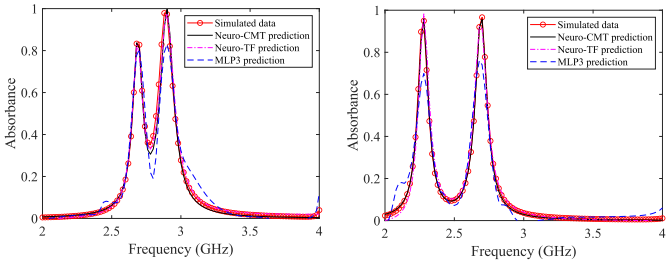

Fig. 9. Comparison between the neuro-CMT, neuro-TF, and MLP3 predictions and the CST simulated data at two selected geometrical samples in Case 2 for $N = 2$. (a) Test sample #1: $[L_1\ L_2\ d] = [22.5\ 20.5\ 53]^T$ (mm). (b) Test sample #2: $[L_1\ L_2\ d] = [22.5\ 27.5\ 18]^T$ (mm).

the neuro-CMT model can be reused to predict the EM response for the metasurface with more resonators in each unit cell, that is, for $N \geq 3$. In other words, due to the incorporation of the multiresonant CMT equations, neuro-CMT does not need to build a parametric model from scratch when the number of resonators changes in each unit cell of the metasurface.

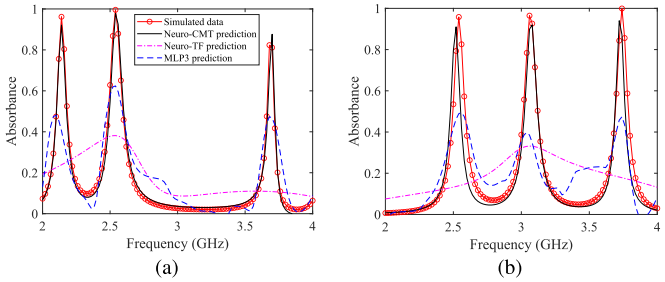

Fig. 10. Comparison between the neuro-CMT, neuro-TF, and MLP3 predictions and the CST simulated data at two selected test samples for $N = 3$. (a) Test sample #1: $\boldsymbol{x} = [13.5\ 29.5\ 24.1667\ 29.6667\ 83.0]^T$ (mm). (b) Test sample #2: $\boldsymbol{x} = [24.1667\ 18.8333\ 13.5000\ 29.6667\ 29.6667]^T$ (mm).

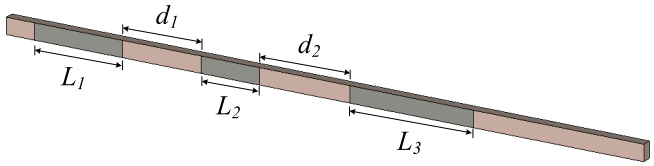

Fig. 11. EM structure of the unit cell for the neuro-CMT-based design of a frequency-selected microwave absorber.

Once the single- and double-resonator neural networks in the proposed neuro-CMT approach are trained, they can be reused to construct neuro-CMT models for multiresonator systems with different numbers of resonators, as long as the unit cell size is not changed. To illustrate this, the neuro-CMT predictions for $N = 3, 4, 5, 6$ are provided in Fig. 8, which cannot be done by the MLP3 and neuro-TF models merely trained with the EM data for $N = 2$. To make MLP3 and neuro-TF be able to do predictions for $N = 3, 4, 5, 6$, new parametric models have to be developed from scratch to model the EM behavior of the corresponding metasurfaces. This will lead to many additional EM simulations and neural network trainings, resulting in a lot of new computational overheads. To better illustrate this, we consider an additional case (i.e., Case 3 in Table II) for $N = 3$ and compare the modeling performance of the three methods, as shown in Table III and Fig. 10. We can see from Fig. 10 that the neuro-CMT prediction matches the EM data much better than the other two methods. More importantly, the neuro-CMT predictions are done without the need of generating any additional EM training samples, while the MLP3 and neuro-TF predictions are done at the cost of over 5000 additional EM training samples.

The modeling results in Figs. 8–10 demonstrate the ability of the neuro-CMT model for predicting the EM response of multiresonator systems at new geometrical parameter values accurately and efficiently. In what follows, we demonstrate how to leverage these advantages to achieve efficient and intelligent metasurface design.

B. Neuro-CMT-Based Design Optimization of Microwave Absorbers

1) Design of a Frequency-Selected Microwave Absorber: We first apply the proposed neuro-CMT approach to the design optimization of a frequency-selected microwave absorber, whose unit cell ($N = 3$) is shown in Fig. 11.

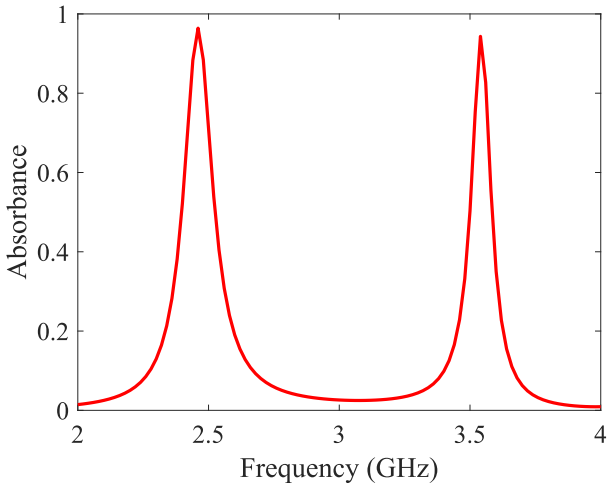

Fig. 12. CST simulated data at the initial design for the frequency-selected absorber.

Five design parameters are considered, that is, $\boldsymbol{x} = [L_1\ L_2\ L_3\ d_1\ d_2]^T$ (mm). We perform EM optimization of three frequency-selected microwave absorbers with different design specifications as follows.

1) *Specifications for Frequency-Selected Absorber #1:* $|\alpha| \geq 0.85$, at specified frequencies of 2.6, 3.0, and 3.3 GHz.
2) *Specifications for Frequency-Selected Absorber #2:* $|\alpha| \geq 0.9$, at specified frequencies of 2.2, 2.8, and 3.4 GHz.
3) *Specifications for Frequency-Selected Absorber #3:* $|\alpha| \geq 0.8$, at specified frequencies of 2.85, 3.3, and 3.5 GHz.

The initial design for optimization is given by $\boldsymbol{x} = [25\ 25\ 15\ 10\ 10]^T$ (mm). The CST simulated data at the initial design is shown in Fig. 12. The quasi-Newton method is employed to solve (16) based on the neuro-CMT surrogate. The neuro-CMT-based optimization takes only about 70 ms to achieve the optimal solution for each absorber. Note that the trained single- and double-resonator neural networks can be reused for these three different design specifications. In other words, there are no additional EM simulations and neural network trainings when a new design specification set is considered. The optimal geometrical parameter values for the three absorbers obtained from the proposed approach are as follows.

1) $\boldsymbol{x}_{\text{opt}}$*#1:* $\boldsymbol{x} = [23.4079\ 19.6273\ 16.8062\ 20.4982\ 20.4850]^T$ (mm).
2) $\boldsymbol{x}_{\text{opt}}$*#2:* $\boldsymbol{x} = [28.4128\ 21.5938\ 16.2422\ 30.0937\ 10.7797]^T$ (mm).
3) $\boldsymbol{x}_{\text{opt}}$*#3:* $\boldsymbol{x} = [15.3671\ 17.0553\ 20.9992\ 24.9899\ 72.5491]^T$ (mm).

The optimal designs are verified by CST full-wave EM simulations as shown in Fig. 13. For the purpose of comparison, we also use CST to perform direct optimization of the frequency-selected absorber with the same initial design parameter values and same design specifications for the three absorbers described above. Table IV illustrates the comparison between the two methods.

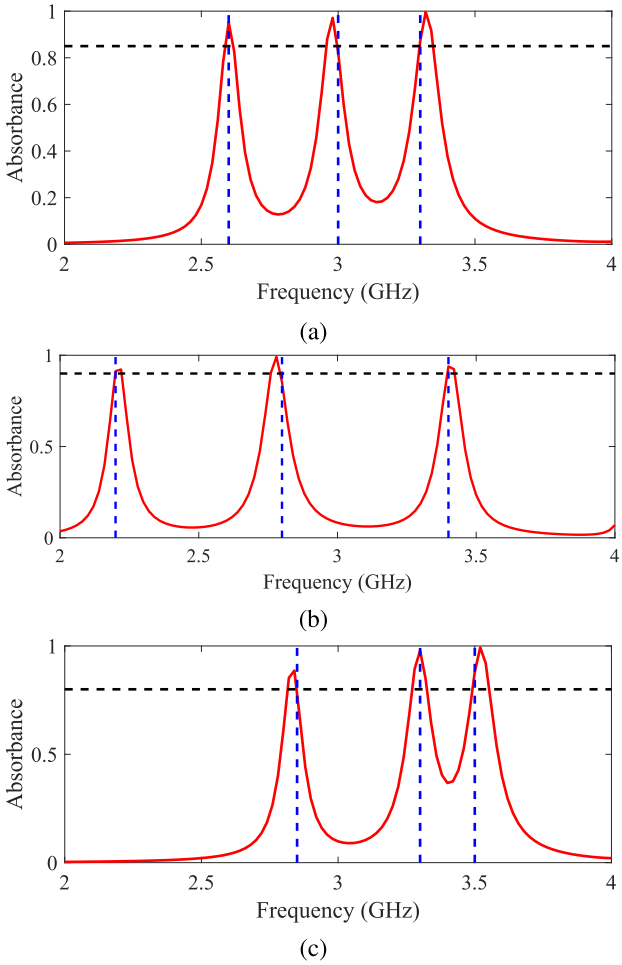

Fig. 13. Absorbance in the magnitude of CST simulated data at (a) $\boldsymbol{x}_{\text{opt}}$#1, (b) $\boldsymbol{x}_{\text{opt}}$#2, and (c) $\boldsymbol{x}_{\text{opt}}$#3, for three different sets of design specifications of the frequency-selected absorber example. The blue and black dashed lines in each figure indicate the corresponding design specification. As can be seen from the figure, the proposed neuro-CMT model behaves well in design optimization with different specifications.

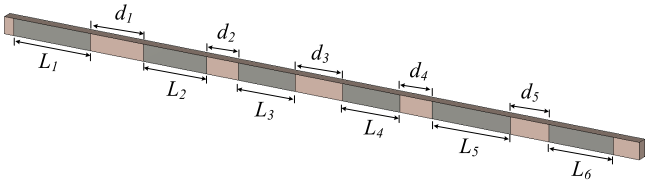

Fig. 14. EM structure of the unit cell for the neuro-CMT-based design of a wideband microwave absorber.

2) Design of a Wideband Microwave Absorber: Next, we apply the proposed neuro-CMT approach to the design optimization of a wideband microwave absorber, whose unit cell (with $N = 6$) is shown in Fig. 14. Eleven design parameters are considered, that is, $\boldsymbol{x} = [L_1\ L_2\ L_3\ L_4\ L_5\ L_6\ d_1\ d_2\ d_3\ d_4\ d_5]^T$ (mm). We perform EM optimization of three wideband microwave absorbers with different design specifications as follows.

1) *Specifications for Wideband Absorber #1:* $|\alpha| \geq 0.75$, in specified frequency range of 2.7–3.3 GHz.
2) *Specifications for Wideband Absorber #2:* $|\alpha| \geq 0.8$, in specified frequency range of 2.8–3.3 GHz.

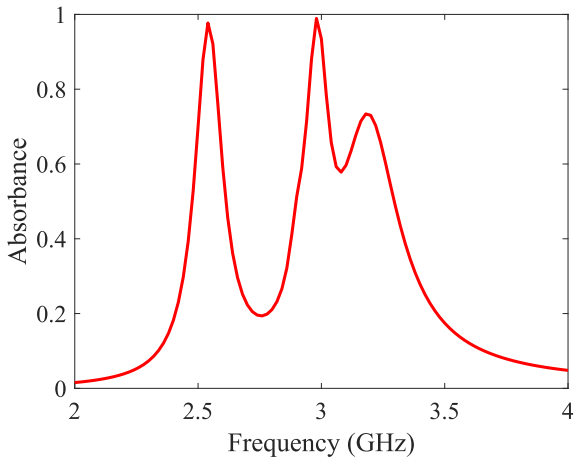

Fig. 15. CST EM data at the initial design for the wideband absorber.

TABLE IV
CPU TIME OF OPTIMIZATIONS FOR THE MICROWAVE ABSORBER EXAMPLES

Different Specifications		Proposed neuro-CMT-Based Optimization	Direct EM Optimization
Frequency-Selected	Specification 1 ($\|\alpha\| \geq 0.85$ at {2.6, 3.0, 3.3} GHz)	10.13 hours (Model Development) + 70 ms (Optimization)	8.6 hours
	Specification 2 ($\|\alpha\| \geq 0.9$ at {2.2, 2.8, 3.4} GHz)	70 ms	7.33 hours
	Specification 3 ($\|\alpha\| \geq 0.8$ at {2.85, 3.3, 3.5} GHz)	70 ms	10.13 hours
Wideband	Specification 1 ($\|\alpha\| \geq 0.75$ in [2.7, 3.3] GHz)	40 s	43.33 hours
	Specification 2 ($\|\alpha\| \geq 0.8$ in [2.8, 3.3] GHz)	40 s	23.52 hours
	Specification 3 ($\|\alpha\| \geq 0.7$ in [2.6, 3.2] GHz)	40 s	31.47 hours
Total		10.16 hours	5 days 4.38 hours

3) *Specifications for Wideband Absorber #3:* $|\alpha| \geq 0.7$, in specified frequency range of 2.6–3.2 GHz.

The initial design for optimization is given by

$$\boldsymbol{x} = [24.5\ 20\ 18\ 18\ 24.5\ 20\ 20\ 10\ 15\ 10\ 12]^T \quad \text{(mm)}.$$

The CST simulated EM data at the initial design is shown in Fig. 15. The proposed neuro-CMT-based optimization takes only about 40 s to achieve the optimal solution for each absorber. The trained single- and double-resonator neural networks can be reused for these three design specifications. In other words, there are no new EM simulations and neural network trainings performed, even though the number of resonators in each unit cell changes from $N = 3$ to $N = 6$. The optimal geometrical parameter values for the three absorbers obtained from the proposed approach are as follows.

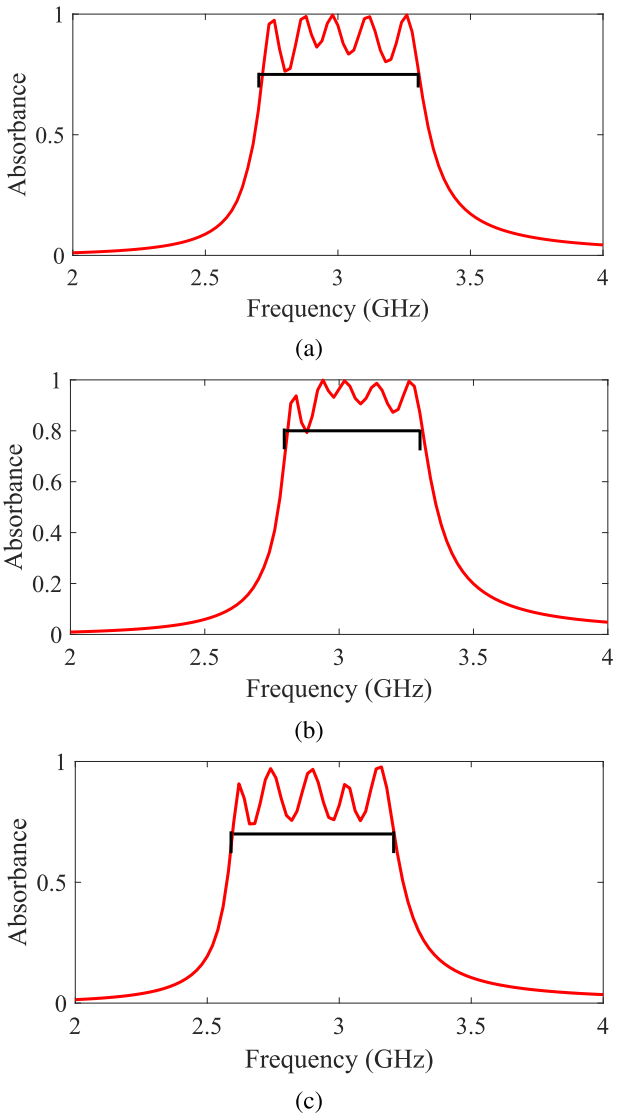

Fig. 16. Absorbance in the magnitude of CST simulated data at (a) $\boldsymbol{x}_{\text{opt}}$#1, (b) $\boldsymbol{x}_{\text{opt}}$#2, and (c) $\boldsymbol{x}_{\text{opt}}$#3, for three different sets of design specifications of the wideband absorber example.

1) $\boldsymbol{x}_{\text{opt}}$*#1:* $\boldsymbol{x} = [18.8427\ 22.0174\ 19.7096\ 17.5663\ 22.4325\ 20.75966.0722\ 5.0\ 6.8052\ 16.7137\ 30.0]^T$ (mm).
2) $\boldsymbol{x}_{\text{opt}}$*#2:* $\boldsymbol{x} = [18.9544\ 20.8490\ 19.2777\ 17.4661\ 21.7993\ 20.1207\ 5.0\ 5.4819\ 7.9761\ 16.0227\ 29.7573]^T$ (mm).
3) $\boldsymbol{x}_{\text{opt}}$*#3:* $\boldsymbol{x} = [23.1704\ 23.2382\ 20.5002\ 18.2843\ 22.3191\ 19.3581\ 26.0211\ 6.3439\ 8.4194\ 18.887\ 8.1669]^T$ (mm).

The optimal design is verified by CST full-wave EM simulation as shown in Fig. 16. For the purpose of comparison, we also use CST to perform direct optimization of the wideband absorber with the same initial design parameter values and same design specifications for the three absorbers described above. Table IV illustrates the comparison between the two methods. For neuro-CMT-based optimization, the model development time is 10.13 h including EM data generation and surrogate model training. Once the training of the neuro-CMT model is done, it can be reused repetitively

for new optimizations. Table IV shows that the total CPU time for model development and absorber design optimization using the neuro-CMT approach is 10.16 h versus 5 days 4.38 h for direct EM optimization. The more we reuse the neuro-CMT model, the more time will be saved.

VII. Conclusion

We have proposed a novel physics-driven machine-learning approach incorporating the CMT to realize fast and intelligent metasurface optimizations. The proposed approach combines the neural network technique with CMT to develop a surrogate model, that is, the neuro-CMT model, which is able to provide fast yet accurate predictions of EM responses of metasurfaces. The trained model has been further exploited to accelerate metasurface design optimizations with different functionalities, including frequency-selected absorbers and wide-band absorbers. The proposed approach paves the way for the development of more advanced intelligent physics-driven ML approaches in metasurface design. In future experimental studies, we would explore the application of the proposed method to facilitate the design of metasurfaces of other types and with more difficult design objectives.

References

[1] T. J. Cui, D. R. Smith, and R. Liu, *Metamaterials: Theory, Design, and Applications*. New York, NY, USA: Springer, 2010.

[2] X. Gao, X. Han, W.-P. Cao, H. O. Li, H. F. Ma, and T. J. Cui, "Ultrawideband and high-efficiency linear polarization converter based on double V-shaped metasurface," *IEEE Trans. Antennas Propag.*, vol. 63, no. 8, pp. 3522–3530, Aug. 2015.

[3] F.-C. Huang, C.-N. Chiu, T.-L. Wu, and Y.-P. Chiou, "A circular-ring miniaturized-element metasurface with many good features for frequency selective shielding applications," *IEEE Trans. Electromagn. Compat.*, vol. 57, no. 3, pp. 365–374, Jun. 2015.

[4] I. Malkiel, M. Mrejen, A. Nagler, U. Arieli, L. Wolf, and H. Suchowski, "Plasmonic nanostructure design and characterization via deep learning," *Light, Sci. Appl.*, vol. 7, no. 1, pp. 1–8, Sep. 2018.

[5] C. C. Nadell, B. Huang, J. M. Malof, and W. J. Padilla, "Deep learning for accelerated all-dielectric metasurface design," *Opt. Exp.*, vol. 27, no. 20, pp. 27523–27535, Sep. 2019.

[6] W. Ma, F. Cheng, and Y. Liu, "Deep-learning-enabled on-demand design of chiral metamaterials," *ACS Nano*, vol. 12, no. 6, pp. 6326–6334, Jun. 2018.

[7] H. P. Wang et al., "Deeping learning designs of anisotropic metasurfaces in ultrawideband based on generative adversarial networks," *Adv. Intell. Syst.*, vol. 2, Sep. 2020, Art. no. 2000068.

[8] S. An et al., "Deep learning modeling approach for metasurfaces with high degrees of freedom," *Opt. Exp.*, vol. 28, no. 21, pp. 31932–31942, 2020.

[9] T. Qiu et al., "Deep learning: A rapid and efficient route to automatic metasurface design," *Adv. Sci.*, vol. 6, pp. 1–12, Jun. 2019.

[10] S. Koziel and M. Abdullah, "Machine-learning-powered EM-based framework for efficient and reliable design of low scattering metasurfaces," *IEEE Trans. Microw. Theory Techn.*, vol. 69, no. 4, pp. 2028–2041, Apr. 2021.

[11] M. Abdullah and S. Koziel, "Supervised-learning-based development of multibit RCS-reduced coding metasurfaces," *IEEE Trans. Microw. Theory Techn.*, vol. 70, no. 1, pp. 264–274, Jan. 2022.

[12] X. Shi, T. Qiu, J. Wang, X. Zhao, and S. Qu, "Metasurface inverse design using machine learning approaches," *J. Phys. D, Appl. Phys.*, vol. 53, May 2020, Art. no. 275105.

[13] Q. Zhang et al., "Machine-learning designs of anisotropic digital coding metasurfaces," *Adv. Theory Simul.*, vol. 2, Feb. 2019, Art. no. 1800132.

[14] L. Li, L. G. Wang, F. L. Teixeira, C. Liu, A. Nehorai, and T. J. Cui, "DeepNIS: Deep neural network for nonlinear electromagnetic inverse scattering," *IEEE Trans. Antennas Propag.*, vol. 67, no. 3, pp. 1819–1825, Mar. 2019.

[15] R. Zhu et al., "Metasurface design by a Hopfield network: Finding a customized phase response in a broadband," *J. Phys. D, Appl. Phys.*, vol. 53, Jul. 2020, Art. no. 415001.

[16] C. Liu, W. M. Yu, Q. Ma, L. Li, and T. J. Cui, "Intelligent coding metasurface holograms by physics-assisted unsupervised generative adversarial network," *Photon. Res.*, vol. 9, no. 4, p. B159, Apr. 2021.

[17] P. Liu, L. Chen, and Z. N. Chen, "Prior-knowledge-guided deep-learning-enabled synthesis for broadband and large phase shift range metacells in metalens antenna," *IEEE Trans. Antennas Propag.*, vol. 70, no. 7, pp. 5024–5034, Jul. 2022.

[18] S. Koziel, N. Calik, P. Mahouti, and M. A. Belen, "Low-cost and highly-accurate behavioral modeling of antenna structures by means of knowledge-based domain-constrained deep learning surrogates," *IEEE Trans. Antennas Propag.*, early access, Oct. 26, 2022, doi: 10.1109/TAP.2022.3216064.

[19] S. Koziel and A. Pietrenko-Dabrowska, "Expedited variable-resolution surrogate modeling of miniaturized microwave passives in confined domains," *IEEE Trans. Microw. Theory Techn.*, vol. 70, no. 11, pp. 4740–4750, Nov. 2022.

[20] S. Koziel, A. Pietrenko-Dabrowska, and U. Ullah, "Low-cost modeling of microwave components by means of two-stage inverse/forward surrogates and domain confinement," *IEEE Trans. Microw. Theory Techn.*, vol. 69, no. 12, pp. 5189–5202, Dec. 2021.

[21] W. Suh, Z. Wang, and S. Fan, "Temporal coupled-mode theory and the presence of non-orthogonal modes in lossless multimode cavities," *IEEE J. Quantum Electron.*, vol. 40, no. 10, pp. 1511–1518, Oct. 2004.

[22] L. Verslegers, Z. Yu, Z. Ruan, P. B. Catrysse, and S. Fan, "From electromagnetically induced transparency to superscattering with a single structure: A coupled-mode theory for doubly resonant structures," *Phys. Rev. Lett.*, vol. 108, no. 8, Feb. 2012, Art. no. 0839021.

[23] S. Yi, M. Zhou, Z. Wang, and Z. Yu, "Superradiant absorption in multiple optical nanoresonators," *Phys. Rev. B, Condens. Matter*, vol. 89, no. 19, pp. 1–7, May 2014.

[24] J. Lin et al., "Tailoring the lineshapes of coupled plasmonic systems based on a theory derived from first principles," *Light, Sci. Appl.*, vol. 9, no. 1, pp. 1–11, Sep. 2020.

[25] R. Audhkhasi, B. Zhao, S. Fan, Z. Yu, and M. L. Povinelli, "Spectral emissivity modeling in multi-resonant systems using coupled-mode theory," *Opt. Exp.*, vol. 30, no. 6, pp. 9463–9472, Mar. 2022.

[26] M. Zhou et al., "Inverse design of metasurfaces based on coupled-mode theory and adjoint optimization," *ACS Photon.*, vol. 8, no. 8, pp. 2265–2273, Aug. 2021.

[27] J. C. Lagarias, J. A. Reeds, M. H. Wright, and P. E. Wright, "Convergence properties of the Nelder–Mead simplex method in low dimensions," *SIAM J. Optim.*, vol. 9, no. 1, pp. 112–147, 1998.

[28] F. Feng, C. Zhang, J. Ma, and Q.-J. Zhang, "Parametric modeling of EM behavior of microwave components using combined neural networks and pole-residue-based transfer functions," *IEEE Trans. Microw. Theory Techn.*, vol. 64, no. 1, pp. 60–77, Jan. 2016.

[29] F. Feng, W. Na, W. Liu, S. Yan, L. Zhu, and Q.-J. Zhang, "Parallel gradient-based EM optimization for microwave components using Adjoint-sensitivity-based neuro-transfer function surrogate," *IEEE Trans. Microw. Theory Techn.*, vol. 68, no. 9, pp. 3606–3620, Sep. 2020.

[30] J. W. Bandler and S. HuaChen, "Circuit optimization: The state of the art," *IEEE Trans. Microw. Theory Techn.*, vol. MTT-36, no. 2, pp. 424–443, Feb. 1988.

[31] Q. J. Zhang, "NeuroModelerPlus," Dept. Electron., Carleton Univ., Ottawa, ON, Canada, 2008.

Jianan Zhang (Member, IEEE) received the B.Eng. degree from Tianjin University, Tianjin, China, in 2013, and the Ph.D. degree from the School of Microelectronics, Tianjin University, and the Department of Electronics, Carleton University, Ottawa, ON, Canada, in 2020.

From 2020 to 2022, he was a Post-Doctoral Research Associate with the Department of Electronics, Carleton University. He is currently an Associate Professor with the State Key Laboratory of Millimeter Waves, Southeast University, Nanjing, China. His research interests include neural network-based electromagnetic (EM) parametric modeling and optimization, surrogate modeling and surrogate-assisted optimization, finite-element analysis in EM, and quantum computing with applications to EM problems.

Jian Wei You (Senior Member, IEEE) received the B.Sc. degree in electrical engineering from Xidian University, Xi'an, China, in 2010, and the Ph.D. degree in the electromagnetic field and microwave techniques from Southeast University, Nanjing, China, in 2016.

From January 2016 to December 2020, he was a Research Associate with the Department of Electronic and Electrical Engineering, University College London, London, U.K. In March 2021, he joined Southeast University, as a Full Professor. His research interests include computational electromagnetic algorithms, microwave and millimeter-wave circuits and antenna simulations, multiphysics and multiscale simulation, plasmonics, topological photonics, and nonlinear optics and quantum information.

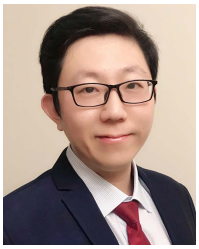

Feng Feng (Senior Member, IEEE) received the B.Eng. degree from Tianjin University, Tianjin, China, in 2012, and the Ph.D. degree from the School of Microelectronics, Tianjin University, and the Department of Electronics, Carleton University, Ottawa, ON, Canada, in 2017.

From 2017 to 2020, he was a Post-Doctoral Fellow with the Department of Electronics, Carleton University. He is currently a Full Professor with the School of Microelectronics, Tianjin University. His research interests include electromagnetic parametric modeling and design optimization algorithms, deep neural network modeling method, space mapping algorithm and surrogate model optimization, the finite-element method in electromagnetic simulation and optimization, and multiphysics modeling and optimization.

Weicong Na (Member, IEEE) received the B.Eng. degree from Tianjin University, Tianjin, China, in 2012, and the Ph.D. degree from the School of Microelectronics, Tianjin University, and the Department of Electronics, Carleton University, Ottawa, ON, Canada, in 2018.

She is currently with the Associate Professor of Information Technology, Beijing University of Technology, Beijing, China. Her research interests include microwave circuit modeling and design, automated neural network model generation algorithm, EM field knowledge-based modeling and optimization, and deep neural network modeling for microwave applications.

Zhuo Chen Lou (Graduate Student Member, IEEE) received the B.Eng. degree from the School of Information Science and Engineering, Southeast University, Nanjing, China, in 2022.

He is currently a Research Assistant with the State Key Laboratory of Millimeter Waves, Southeast University. His research interests include computational electromagnetic algorithms, microwave and millimeter-wave circuits, and antenna simulations.

Qi-Jun Zhang (Fellow, IEEE) received the B.Eng. degree from the Nanjing University of Science and Technology, Nanjing, China, in 1982, and the Ph.D. degree in electrical engineering from McMaster University, Hamilton, ON, Canada, in 1987.

From 1982 to 1983, he was with the System Engineering Institute, Tianjin University, Tianjin, China. From 1988 to 1990, he was with Optimization Systems Associates (OSA) Inc., Dundas, ON, Canada, where he developed advanced microwave optimization software. In 1990, he joined the Department of Electronics, Carleton University, Ottawa, ON, Canada, where he is currently a Chancellor's Professor. He has authored or coauthored over 300 publications. He has authored *Neural Networks for RF and Microwave Design* (Artech House, 2000), coedited *Modeling and Simulation of High-Speed VLSI Interconnects* (Kluwer, 1994), and contributed to the Encyclopedia of *RF and Microwave Engineering* (Wiley, 2005), *Fundamentals of Nonlinear Behavioral Modeling for RF and Microwave Design* (Artech House, 2005), and *Analog Methods for Computer-Aided Analysis and Diagnosis* (Marcel Dekker, 1988). His research interests include microwave design automation, especially neural networks and optimization methods for high-speed/high-frequency circuit design.

Dr. Zhang is a Fellow of the Electromagnetics Academy and the Canadian Academy of Engineering. He is the Chair of the Technical Committee on Design Automation (MTT-2) of the IEEE Microwave Theory and Techniques Society (IEEE MTT-S). He is an Associate Editor of the IEEE Transactions on Microwave Theory and Techniques. He was a Guest Coeditor for the "Special Issue on High-Speed VLSI Interconnects" for the *International Journal of Analog Integrated Circuits and Signal Processing* (Kluwer, 1994) and twice was a Guest Editor for the "Special Issue on Applications of ANN to RF and Microwave Design" for the *International Journal of RF and Microwave Computer-Aided Engineering* (Wiley, 1999 and 2002).

Tie Jun Cui (Fellow, IEEE) received the B.Sc., M.Sc., and Ph.D. degrees from Xidian University, Xi'an, China, in 1987, 1990, and 1993, respectively.

In March 1993, he joined the Department of Electromagnetic Engineering, Xidian University, and was promoted to Associate Professor in November 1993. From 1995 to 1997, he was a Research Fellow with the Institut fur Hochstfrequenztechnikund Elektronik (IHE), University of Karlsruhe, Karlsruhe, Germany. In July 1997, he joined the Center for Computational Electromagnetics, Department of Electrical and Computer Engineering, University of Illinois at Urbana–Champaign, Champaign, IL, USA, first as a Post-Doctoral Research Associate and then as a Research Scientist. In September 2001, he was a Cheung-Kong Professor with the Department of Radio Engineering, Southeast University, Nanjing, China, where he became the Chief Professor in January 2018. He is the first author of the books *Metamaterials: Theory, Design, and Applications* (Springer, November 2009), *Metamaterials: Beyond Crystals, Noncrystals, and Quasicrystals* (CRC Press, March 2016), and *Information Metamaterials* (Cambridge University Press, 2021). He has authored over 600 peer-reviewed journal articles, which have been cited more than 52 000 times (H-Factor 115; Google Scholar), and licensed over 150 patents.

Dr. Cui received a Research Fellowship from the Alexander von Humboldt Foundation, Bonn, Germany, in 1995, received the Young Scientist Award from the International Union of Radio Science in 1999, was awarded a Cheung Kong Professor by the Ministry of Education, China, in 2001, and received a fellowship from the National Science Foundation of China for Distinguished Young Scholars in 2002. He received the Natural Science Award (first class) from the Ministry of Education, China, in 2011, and the National Natural Science Awards of China (second class, twice) in 2014 and 2018. His research has been selected as one of the most exciting peer-reviewed optics research "Optics in 2016" by *Optics and Photonics News Magazine*, Ten Breakthroughs of China Science in 2010, and many Research Highlights in a series of journals. His work has been widely reported by *Nature News*, *MIT Technology Review*, *Scientific American*, *Discover*, and *New Scientists*. He is an Academician of the Chinese Academy of Sciences. He served as an Associate Editor for the IEEE TRANSACTIONS ON GEOSCIENCE AND REMOTE SENSING and a Guest Editor of *Science China-Information Sciences*, *Science Bulletin*, the IEEE JOURNAL ON EMERGING AND SELECTED TOPICS IN CIRCUITS AND SYSTEM (JETCAS), and *Research*. He is the Chief Editor of Metamaterial Short Books in Cambridge University Press, the Editor of *Materials Today Electronics*, the Associate Editor of *Research*, and an Editorial Board Member of *National Science Review*, *eLight*, *PhotoniX*, *Advanced Optical Materials*, *Small Structure*, and *Advanced Photonics Research*. He presented more than 100 keynote and plenary talks at academic conferences, symposiums, or workshops. From 2019 to 2021, he was ranked in the top 1% for the highly cited articles in the field of Physics by Clarivate Web of Science (Highly Cited Researcher).